

LOCAL POSTBUCKLING ANALYSIS OF CURVED AEROSPACE STRUCTURES

Marc Fischer, David Kennedy

Cardiff School of Engineering, Cardiff University, PO Box 686,
The Parade, Cardiff CF24 3TB, United Kingdom
Email: FischerM@cf.ac.uk

Abstract

Minimum mass design of aerospace structures is greatly enhanced by allowing for their postbuckling reserve of strength, which is mainly due to stress re-distribution within the structure following buckling in a local mode. The paper first outlines a geometrically non-linear analysis for longitudinally compressed panels, in which the ratio of postbuckling to prebuckling axial stiffness is established by an iterative procedure, critical buckling loads and mode shapes being found by an 'exact strip' algorithm. The analysis is illustrated by its application to a simply supported, curved, stiffened panel. The paper next describes an incremental approach to the local postbuckling analysis of longitudinally stiffened cylindrical shells loaded by longitudinal compression and/or a bending moment. The shell is modelled as a collection of skin/stiffener portions, for each of which the critical buckling load and stiffness ratio are determined. Next the axial loads in each portion due to the applied loads are calculated under linear elastic assumptions, so that it is possible to determine which portion will buckle first. Thereafter the buckled portion is modelled with a reduced stiffness, so that the location of the shell's neutral axis changes and is found by an iterative improvement to a method originally developed by Bruhn.

1 Introduction

Aerospace structures such as longitudinally stiffened panels can often carry loads far in excess of their critical buckling loads. This

postbuckling reserve of strength is mainly due to stress re-distribution within the structure following buckling in a local mode and, if allowed for in minimum mass design, can make a valuable contribution to the overall efficiency of such structures.

This paper first outlines a geometrically non-linear analysis for perfect or imperfect longitudinally compressed prismatic plate assemblies [1]. Critical buckling loads and mode shapes are found by the 'exact strip' algorithm of the analysis and optimum design software VICONOPT [2]. The analysis is illustrated by its application to a simply supported, longitudinally stiffened, curved aerospace panel.

Based on a hand calculation method by Bruhn [3], a method has been developed to estimate the postbuckling reserve strength of longitudinally stiffened cylindrical shells, such as fuselage sections. Such structures usually have repetitive cross-sections and can be analysed efficiently by modelling a small number of repeating portions, to match the varying geometric and material properties around the circumference of the fuselage.

If the shell is subjected to bending, more and more portions will buckle as the bending moment increases. Increasing loads are supported by stress re-distributions which will occur across the whole structure. After buckling, the buckled portions will have a reduced load carrying capacity, which can be accounted for by using reduced Young's moduli estimated from VICONOPT postbuckling analyses for each portion.

A model of a longitudinally stiffened cylindrical shell was set up and a postbuckling

analysis carried out. The initial buckling load was exceeded by a significant factor before failure, which points towards the savings in mass which could be achieved when designing such structures.

The method presented in this paper was developed, as part of a final year undergraduate project, to provide a quick first estimate of the load carrying capacity, and benefits from reduced modelling and computation time. It is however not intended to provide the accuracy of a full non-linear finite element analysis.

2 VICONOPT

2.1 General Overview

VICONOPT is a prismatic plate analysis and optimum design computer program [2], which incorporates the earlier programs VIPASA (Vibration and Instability of Plate Assemblies including Shear and Anisotropy) [4] and VICON (VIPASA with Constraints) [5].

VICONOPT covers buckling, postbuckling and vibration of prismatic plate assemblies, and provides an efficient design tool in structural optimisation. For any longitudinally invariant loading combination (of longitudinal, transverse, in-plane shear and pressure loads), critical buckling loads, undamped natural frequencies and mode shapes can be found. Typical sections which VICONOPT can analyse are shown in Figure 1, and a typical component plate showing in-plane loading in Figure 2.

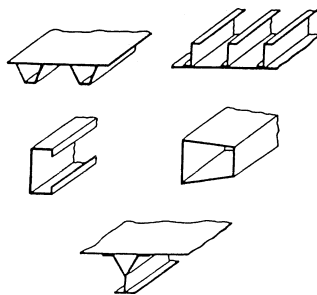


Figure 1. Typical sections which VICONOPT can analyse.

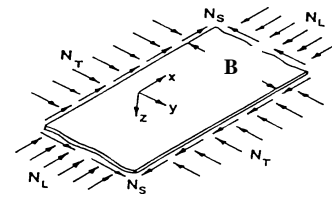


Figure 2. Component plate showing in-plane loading.

2.2 Postbuckling Analysis using VICONOPT

VICONOPT includes a geometrically non-linear analysis in order to investigate the postbuckling behaviour of perfect or imperfect longitudinally compressed prismatic plate assemblies, with local buckling modes [1]. The analysis includes an iterative procedure to determine the ratio of postbuckling to prebuckling axial stiffness K^*/K , and the relationship between applied load P and longitudinal end-shortening strain ϵ_x well into the postbuckling region. The overall accuracy of the postbuckling results is improved by taking into account the stabilising effects of the transverse tension developed in the central portion of a plate whose longitudinal edges are constrained to remain straight. The analysis is based on the assumption that the panel has simply supported ends, and buckles locally with a half-wavelength λ that divides exactly into the panel length ℓ . The method allows for prismatic plate assemblies having a general cross-section. As illustrated in Figure 3, each component plate is divided into n_s longitudinal strips of equal width $b_s=B/n_s$, where B is the

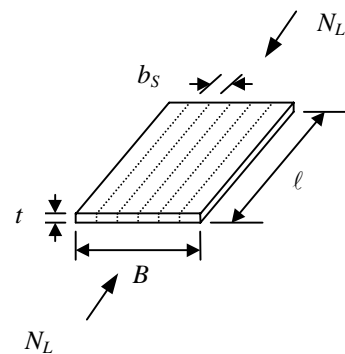


Figure 3. Typical flat plate of width B , subdivided into n_s strips of width $b_s=B/n_s$.

width of the plate. Material properties can be either isotropic or anisotropic, and uniform thickness is assumed across each plate. The analysis optionally allows for geometric shape imperfections with maximum out-of-plane displacement γ_0 . Restricting attention to a single plate (for simplicity), the initial stress resultants are calculated for each strip as

$$N_{xs} = N_L = \frac{P}{B} \quad (1)$$

The iterative procedure of the non-linear analysis consists of a pre-defined number of cycles, each defined by a maximum out-of-plane displacement γ_2 . At the start of each new cycle, γ_2 is incremented by a pre-defined amount. During each cycle, the applied load P and the longitudinal end-shortening strain ϵ_x which correspond to the displacement γ_2 are determined. This process requires a number of iterations to yield convergence, due to changes in the postbuckling mode shape and stress distribution across the cross-section of the structure.

At the start of each iteration, the buckling load P_c and mode shape (of amplitude γ_2) for a perfect structure with the present stress distribution are found. Imperfections are assumed to have the same shape as the buckling mode but an amplitude of γ_0 , so that the applied load P for the imperfect structure is

$$P = (1 - \frac{\gamma_0}{\gamma_2})P_c \quad (2)$$

For the first iteration of the second and all subsequent cycles, the buckling load, mode shape and applied load calculations are replaced by estimated values, derived from the converged results from the previous cycle. The longitudinal strain due to the applied load P is P/S_1 , where

$$S_1 = B(A_{11} - \frac{A_{12}^2}{A_{22}}) \quad (3)$$

The longitudinal strain ϵ_{x0} at the initial buckling load P_{C0} is thus given by

$$\epsilon_{x0} = \frac{P_{c0}}{S_1} \quad (4)$$

For the plate shown in Figure 4, the change in projected length of a linear element of length dx in the longitudinal direction due to a displacement w_2 is given by $\frac{1}{2}(\frac{\partial w_2}{\partial x})^2 dx$. The flexural strain ϵ_{Fx} due to bending of an imperfect plate with half-wavelength λ is thus given by taking the difference between the final and initial projected lengths, as

$$\epsilon_{Fx} = \frac{1}{2\lambda} \int_0^\lambda \left[\left(\frac{\partial w_2}{\partial x} \right)^2 - \left(\frac{\partial w_0}{\partial x} \right)^2 \right] dx + \frac{1}{2\lambda} \int_0^\lambda \left[\left(\frac{\partial v_2}{\partial x} \right)^2 - \left(\frac{\partial v_0}{\partial x} \right)^2 \right] dx \quad (5)$$

Here the displacement v (in the global y direction) has been included as well as w , to allow for the arbitrary alignment of plates in a stiffened panel.

Assuming sinusoidal variations of the modal displacements along any longitudinal line, i.e.

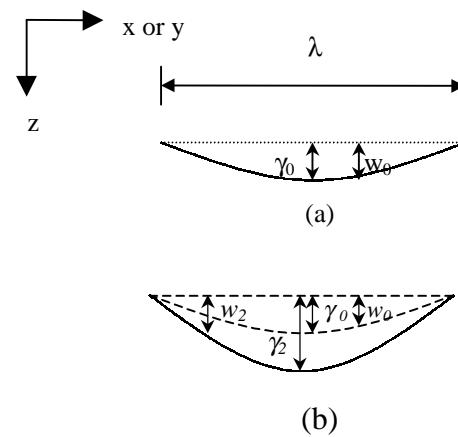


Figure 4. Cross-section of thin rectangular plate having an initial imperfection w_0 with maximum value γ_0 . (a) Unloaded. (b) Loaded.

$$w_2 = \bar{w}_2 \sin\left(\frac{\pi x}{\lambda}\right) \quad (6)$$

equation (5) can be evaluated to give

$$\varepsilon_{F_x} = \left(\frac{\pi^2}{4\lambda^2}\right) (\bar{w}_2^2 + \bar{v}_2^2 - \bar{w}_0^2 - \bar{v}_0^2) \quad (7)$$

the overbars denoting the amplitudes. The stress resultant for flexure is then given by

$$N_{F_x} = \frac{\varepsilon_{F_x} S_1}{B} \quad (8)$$

After buckling has occurred, stress redistribution takes place in the plate, as illustrated in Figure 5. The average stress resultant is $N_L (=P/B)$. At the edges, the stress resultant due to flexure is zero and the stress is taken as

$$S_2 N_L = N_L \left(1 + \frac{1}{P} \sum_s (b_s N_{F_{xs}})\right) \quad (9)$$

where $N_{F_{xs}}$, the stress resultant due to flexure for strip s , is taken as the mean of the values of N_{F_x} at the two edges of the strip. The overall stress resultant N_{xs} in a strip is given by

$$N_{xs} = S_2 N_L - N_{F_{xs}} \quad (10)$$

Convergence within each cycle is based on finding a consistent estimate of the applied load P . On convergence, the end shortening strain ε_x due to the applied load and postbuckling mode is given by

$$\varepsilon_x = \frac{S_2 P}{S_1} \quad (11)$$

The ratios P/P_{C0} and $\varepsilon_x/\varepsilon_{x0}$ from each cycle are plotted to determine the ratio of postbuckling to prebuckling axial stiffness K^*/K .

Prior to the commencement of each new cycle the imperfection shape is altered to that of the latest converged mode, representing the

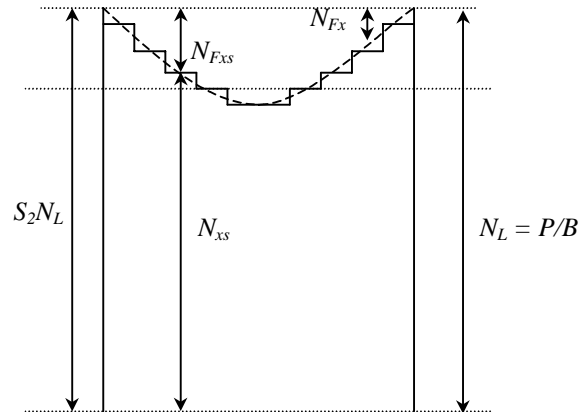


Figure 5. Typical variation of stress resultants across a plate.

worst possible shape. While the amplitude of the imperfection remains unaltered, the postbuckling mode is re-scaled using an increased value of γ_2 for the maximum out-of-plane displacement. An estimated buckling load is then obtained by straight line extrapolation through the converged values of P_C and γ_2 from the last two cycles, and used in place of P_C in equation (2) to estimate the applied load for the first iteration of the next cycle.

3 Postbuckling Analysis of a Curved Aerospace Panel

To illustrate the postbuckling analysis of VICONOPT, consider the simply supported, curved, longitudinally stiffened panel shown in Figure 6(a). The panel is of finite width with five longitudinal stiffeners. The length of the panel is 300mm and simple supports are assumed along all four edges. The distance across the skin between the longitudinal supports and stiffeners is 25mm, and that between adjacent stiffeners is 50mm. The stiffeners are all of the same geometry and size, the web being 15mm deep and the flange 5mm wide. Adjacent stiffeners are inclined at 2 degrees to each other. The thicknesses of the skin and stiffener plates are 1mm and 0.5mm, respectively. The isotropic material used for skin and stiffeners has Young's modulus $E=110\text{GPa}$ and Poisson's ratio $\nu=0.3$.

Given the regular geometry of the panel, use can be made of VICONOPT's repetitive analysis, so that the panel is divided into five of the repeating portions shown in Figure 6(b). The curvature of the skin can be modelled by dividing the skin into a number of flat plates, each being rotated through an appropriate angle. The higher the number of skin plates used, the more accurate the representation of the skin curvature. To investigate how the buckling and postbuckling behaviour varied with increasing accuracy of the model, the repeating portion was modelled three times, with four, six and eight skin plates, respectively. The buckling analysis gave a critical mode shape with a half-wavelength of $\lambda=50\text{mm}$ which corresponds to six half-wavelengths along the length of the plate. This mode had a transverse response in which the mode shape was reversed in adjacent repeating portions, see Figure 6(c). The critical buckling loads for the three cases were very similar, at approximately 10.1kN, and the postbuckling analyses showed that the ratios of postbuckling to prebuckling stiffness were almost identical at $K^*/K=0.6$, see Figure 7.

Due to the moderate curvature of the panel, refining the model to more accurately match the curvature of the skin did not have any significant effect on the results. This would be different for sections with higher curvatures. However, for many aerospace structures, such as fuselage panels, the curvature of an individual portion is fairly small, and it is therefore reasonable to model the skin using only a small number of plates. This reduces the computational effort required for postbuckling analyses.

4 Postbuckling Analysis of Longitudinally Stiffened Cylindrical Shells

4.1 Procedure

Using the approach described in section 3, a longitudinally stiffened cylindrical shell can be represented in terms of one or more repeating portions. The structural behaviour of the cylindrical shell will be governed by the

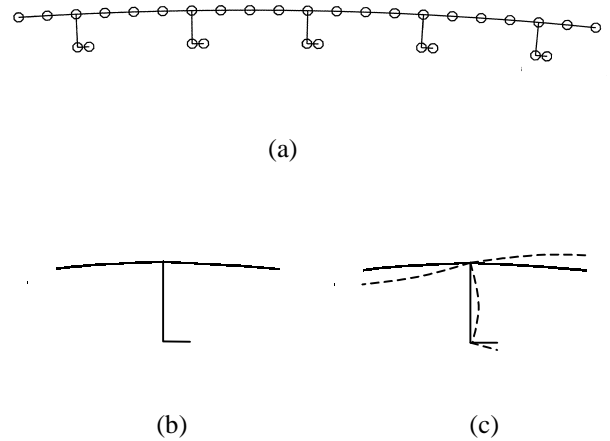


Figure 6. Simply supported, curved, stiffened panel. (a) Cross-section of the panel, showing plate junctions for the model with four skin plates between stiffeners. (b) Cross-section of repeating portion. (c) Initial buckling mode.

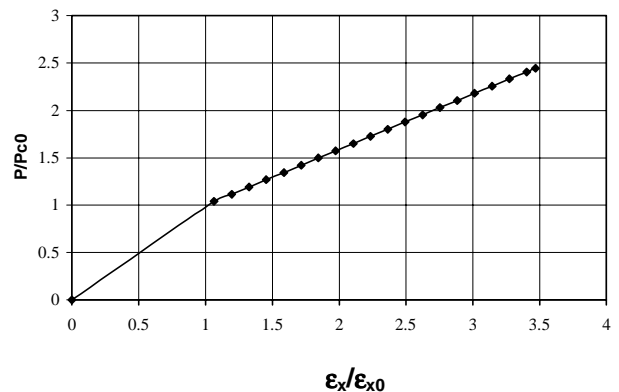


Figure 7. Non-dimensional plot of axial load P against end shortening strain ϵ_x , for a simply supported, curved, stiffened panel. P_{C0} and ϵ_{x0} are the values at initial buckling.

buckling and postbuckling behaviour of the individual portions. Once a portion has buckled, it will have a reduced capacity to resist any further loading. This can be expressed by using either the concept of effective width [6] or reduced E values. For the proposed analysis the latter will be used.

It can be observed that a local reduction in stiffness will lead to a shift in the position of the overall neutral axis. An increasing number of buckled portions in the bottom half of a cylindrical shell subjected to bending would result in the neutral axis moving upwards.

Ultimate failure can be anticipated to occur due to either crippling or yielding of one of the portions.

The position of each portion i can be determined in terms of an angle θ_i through which it has been rotated about the co-ordinate origin, the positive z -axis defining zero degrees (Figure 8). The cross-sectional area A_i of each portion is calculated, as well as the total cross-sectional area. For each component plate j of portion i , the centroid and its distance from the co-ordinate origin are established. The position of the portion's neutral axis z_{NAi} can then be calculated by

$$z_{NAi} = \frac{\sum_{j=1}^n J_{ij}}{\sum_{j=1}^n A_{ij}} \quad (12)$$

where A_{ij} is the cross-sectional area of component plate j , J_{ij} is its first moment of area and n is the number of component plates in portion i . For each portion, the individual section properties and their contribution to the overall section properties of the cylindrical shell need to be determined at each stage of the analysis. The first and second moments of area of each portion relative to the neutral axis of the overall structure will change with the position of this neutral axis. This in turn is affected by the buckling of individual portions and their reduced Young's moduli E_i within the postbuckling region.

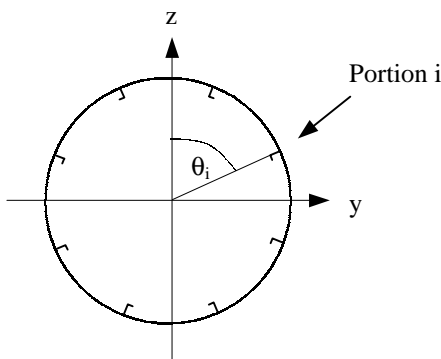


Figure 8. Typical cross-section of a longitudinally stiffened cylindrical shell.

An iterative procedure is required to enable convergence on the changed position of the neutral axis. The difference between the previous and new positions of the neutral axis can be obtained from

$$z_{diff} = \frac{\sum_{i=1}^m E_i J_i}{\sum_{i=1}^m E_i A_i} \quad (13)$$

where A_i is the cross-sectional area of portion i , J_i is its first moment of area about the previous neutral axis and m is the number of portions around the circumference. z_{diff} is taken as a correction factor to be subtracted from the z co-ordinates previously determined for each portion. If z_{diff} is negative (positive), the actual position of the neutral axis lies below (above) the previous position.

Once the position of the neutral axis has been determined, it is then possible to calculate the loading corresponding to the stress level in each portion. The stresses in a portion result from the application of both axial loads and bending moments to the cylindrical shell. Each of these can be divided into dead and live components, the latter being multiplied by increasing load factors F to investigate the postbuckling behaviour of the structure. The total axial load and bending moment are given by

$$\left. \begin{aligned} P &= P_D + FP_L \\ M &= M_D + FM_L \end{aligned} \right\} \quad (14)$$

where the subscripts D and L denote dead and live values, respectively. The strain in each portion can be calculated (approximately) as

$$\epsilon_i = \epsilon_0 - \kappa_0 z_i \quad (15)$$

where z_i is the distance between the centroid of the portion and the neutral axis of the shell, ϵ_0 is the strain due to the axial compression and κ_0 is the curvature due to bending. Denoting the

second moment of area of portion i by I_i , ε_0 and κ_0 are obtained from

$$\left. \begin{aligned} \varepsilon_0 &= \frac{P_D + FP_L}{\sum_{i=1}^m E_i A_i} \\ \kappa_0 &= \frac{M_D + FM_L}{\sum_{i=1}^m E_i I_i} \end{aligned} \right\} \quad (16)$$

which follow directly from Hooke's law. Up to the point of initial buckling, the full moduli of elasticity, denoted \bar{E}_i , should be used for E_i and the stress-strain relationship follows the usual linear curve. However, beyond initial buckling the ensuing non-linear relationship can be accounted for by introducing reduced moduli of elasticity $E_i = \alpha_i \bar{E}_i$ for portions which have buckled, while using the full modulus $E_i = \bar{E}_i$ for those portions which have not buckled. The factors α_i are the ratios of postbuckling to prebuckling axial stiffness K^*/K . They are obtained by performing a separate VICONOPT postbuckling analysis on each repeating portion i and finding the gradient of the P/P_{C0} versus $\varepsilon_v/\varepsilon_{x0}$ curve beyond the point (1,1), see Figure 7.

The load in each portion is next calculated as

$$P_i = E_i A_i \varepsilon_i \quad (17)$$

Knowing the critical buckling loads P_{cri} for each portion from the VICONOPT analysis, the critical load factor F_{cri} can be derived from

$$F_{cri} = \frac{P_{cri}(E_i A_i)^{-1} - P_D (\sum_{k=1}^m E_k A_k)^{-1} + z_i M_D (\sum_{k=1}^m E_k I_k)^{-1}}{P_L (\sum_{k=1}^m E_k A_k)^{-1} - z_i M_L (\sum_{k=1}^m E_k I_k)^{-1}} \quad (18)$$

The lowest such load factor which would cause initial or further buckling is selected. This factor is then applied to calculate an increased

axial load and bending moment, and the process described above is repeated.

From the material properties of the skin and stiffener, the loading which would cause yielding of a repeating portion can be determined. At the beginning of each stage, the current loading in each portion is checked against this yield load. Once yielding has occurred, the portion cannot support any further loading and the structure is deemed to fail.

The procedure presented, which has been coded in FORTRAN90, does not allow for the stabilising effects due to possible frame spacing which would have to be taken into account when analysing shell structures such as fuselage sections. However VICONOPT is capable of analysing sections with beam supporting structures [2], and appropriate enhancements could be readily included in the method.

The computer program consists of a series of stages. During the first stage, the material properties and all the relevant data on the geometry of the portions and overall structure are read in from an input file. The cross-sectional area, the distance between the centroid of the portion and the neutral axis, and the first and second moments of area are determined for each portion.

Initially, the overall neutral axis is assumed to pass through the co-ordinate origin at the centre of the cross-section. This is only true for cross-sections which are symmetric about the centre and have uniform material properties. If some parts of the shell needed to be stiffer than others, this would lead to the position of the neutral axis being off-centre. Following the above iterative procedure, the true position of the neutral axis is determined. Convergence is based on a pre-defined tolerance on the difference between the previous and new positions of the neutral axis. Unless otherwise specified by the user, this tolerance is set to be 0.5% of the radius.

Once the initial position of the neutral axis has been determined, assuming a linear variation of the stresses due to the bending moment through the depth of the shell section

and a uniform stress distribution due to the overall axial load, the loads P_i on each portion and the corresponding load factors F_{cri} to give critical conditions are determined. Since no portions are assumed to have buckled during stage 1, all these calculations involve the full Young's moduli \bar{E}_i . The load factor which causes buckling of the first portion is determined and stage 2 is entered, with the live loads on the structure being increased by this factor.

The assumptions made in stage 1 regarding the stress distributions across the structure are no longer valid, since buckling has occurred. Stress re-distributions across the section need to be taken into account by using the reduced modulus E_i for the portion(s) concerned, which gives the earlier described shift in neutral axis. Repeating the procedure of stage 1, the next higher load factor to cause further buckling is determined, and the next stage is entered.

The process is repeated until one of the stopping criteria (i.e. crippling or yielding) is met.

4.2 Example Problem

A longitudinally stiffened cylindrical shell was modelled with the dimensions and material properties given in Table 1. For simplicity, the material properties of skin and stiffeners were taken to be the same, and the skin thickness was taken to be constant around the circumference of the shell section.

Given a diameter of 6.0m and a stiffener spacing of 184mm, the total number of stiffeners required was 102. The assumption was made that the stiffeners were equally spaced and symmetrically distributed around the cross-section. In total, three different types of repetitive portions (S1, S2 and S3) were modelled, with stiffeners varying in size as indicated in Table 1. The sequence of portions around the cross-section is shown in Figure 9. Thus the top of the shell had lower stiffness than the bottom.


Length	4500 mm		
Radius	3000 mm		
Skin Thickness	1.0 mm		
Material	$E=72.5\text{GPa}$ $\sigma_y=410\text{MPa}$		
Stiffener Spacing	184 mm		
Stiffener Shape			
No. of Stiffeners	102		
Stiffener Dimensions (mm)	S1	S2	S3
Web depth	22.23	25.40	28.50
thickness	0.89	1.27	1.52
Flange depth	14.30	17.50	20.60
thickness	0.89	1.27	1.52
Cross-sectional Area of Portion (mm²)	S1	S2	S3
	220	240	260
Critical Buckling Load (N)	S1	S2	S3
λ	$\ell/44$	$\ell/44$	$\ell/45$
$\alpha_c=K^*/K$	0.525	0.582	0.621

Table 1. Longitudinally stiffened cylindrical shell data.

For the VICONOPT models of the repetitive portions, the curvature of the skin of each portion was approximated by six flat plates, each inclined at an angle of 0.588 degrees to its neighbours. However, single plates of width 92.7mm were assumed for the subsequent analysis.

The cylindrical shell section was chosen to have an arbitrary length $\ell=4.5\text{m}$. The effects of varying lengths on the postbuckling behaviour and ultimate failure mode would need to be investigated further.

Table 1 shows that the VICONOPT buckling and postbuckling analyses resulted in similar behaviour for all three portions. However, while the critical buckling modes for

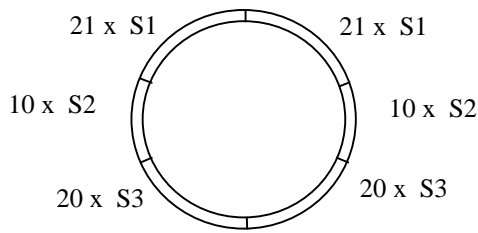


Figure 9. Distribution of repeating portions around the circumference.

portions S1 and S2 had a half-wavelength of $\lambda = \ell/44$, the critical value of λ for portion S3 was $\ell/45$. For compatibility reasons, it was necessary to decide on a single value for all three portions; $\lambda = \ell/44$ was chosen, since portions S1 and S2 buckle at lower critical loads than portion S3. The effects of mode interaction and mode changes within the postbuckling region were not considered as part of this work.

There are several ways of estimating the gradient K^*/K after the onset of buckling. VICONOPT postbuckling results give the slope between each point on the postbuckling curve and the point of initial buckling. To find an overall estimate of the gradient, the average slope could be considered, or (more conservatively) the gradient of the secant passing through the point of initial buckling and the highest point reached in the postbuckling region. For this problem, an average value was found to provide sufficient accuracy.

For the postbuckling analysis of the cylindrical shell, axial loads applied to the section were neglected and only the bending moment was taken into account. The moment was applied in such a way that the bottom of the shell went into compression and the top went into tension. With no portions buckled during stage 1, this resulted in a typical linear load distribution, varying from maximum tension at the top to maximum compression at the bottom, with no loading at the neutral axis (Figure 10). The cross-sectional areas of the individual portions were assumed to remain constant, and thus working with total axial loads instead of stresses could be justified.

The analysis showed good convergence on the position of the neutral axis with the accuracy level set to 10^{-4} m. The position of the neutral axis moved upwards with an increasing number of buckled portions at the bottom of the shell. Each stage resulted in buckling of further critical portions, located symmetrically starting at the bottom of the shell. The reduced stiffness after buckling is reflected by the change in gradient of the load distribution curve for the shell section (Figure 10).

Since an average reduction factor had been estimated for each portion from the VICONOPT results, once critical buckling was exceeded, the reduced gradient of the load distribution curve remained constant for each type of portion.

From Figure 10 it can be seen how an increase in overall load leads to more and more buckled portions. The α_i used to obtain the reduced Young's modulus E_i of each portion result in the changes in gradients which can be identified in Figure 10.

Overall, the analysis showed that the shell model had a significant postbuckling reserve of strength. Initial buckling occurred at a bending moment of 884.6MNm. For 46 portions to buckle, this was increased by a factor of 2.4 to 2120.7MNm, with no yielding in any of the portions. With almost half of the portions buckled, this points towards the overall postbuckling reserve of strength of the structure and the significant scope for improving the overall efficiency.

5 Conclusions

Longitudinally stiffened panels often possess a substantial postbuckling reserve of strength, which is mainly due to stress re-distribution following buckling in a local mode. The critical buckling load and the ratio of postbuckling to prebuckling axial stiffness of a simply supported, curved, stiffened panel have been obtained using a recent extension to the exact strip algorithm of the buckling software VICONOPT into the initial postbuckled region.

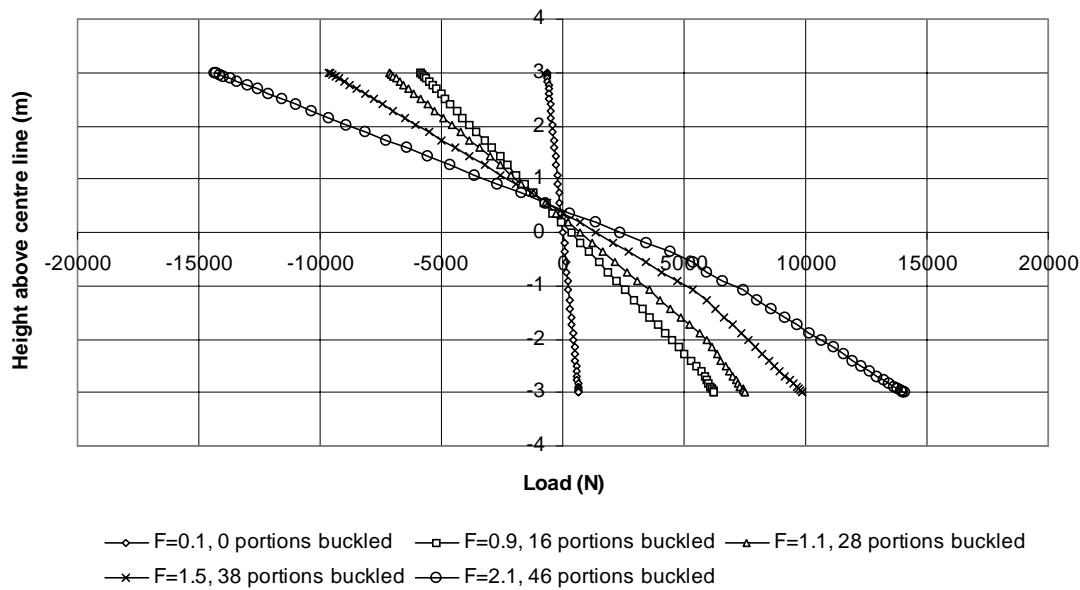


Figure 10. Postbuckling analysis of a longitudinally stiffened cylindrical shell: load distribution (compression positive).

A method has been presented in which a fuselage section is modelled as a longitudinally stiffened cylindrical shell comprising a collection of repeating skin/stiffener portions, for each of which the critical buckling load and axial stiffness ratio are obtained using VICONOPT. When the shell is loaded by longitudinal compression and/or a bending moment, the axial loads in each portion are first determined under linear elastic assumptions, so that it is possible to determine which portion will buckle first. The postbuckling behaviour is then studied using an incremental approach in which buckled portions are modelled with a reduced stiffness, so that the location of the shell's neutral axis changes and is found by an iterative improvement to a method originally developed by Bruhn.

Results for a fuselage section with three different types of repeating portions demonstrated a postbuckling reserve of strength such that no yielding occurred before 46 of the 102 portions had buckled, at which point the applied bending moment was 2.4 times that which caused initial buckling of the first portion. This result suggests that allowing for the postbuckling reserve in minimum mass design can achieve significant improvements in the overall efficiency of such a structure.

Acknowledgements

The first author is grateful for the support and advice received from Mr. David Fitzsimmons during his summer placements at DaimlerChrysler Aerospace Airbus GmbH (Hamburg) in 1998 and 1999.

References

- [1] Powell SM, Williams FW, Askar A-S and Kennedy D. Local postbuckling analysis for perfect and imperfect longitudinally compressed plates and panels. *Proc. of 39th AIAA/ASME/ASCE/AHS/ASC Structures, Structural Dynamics, and Materials Conference*, Long Beach, CA, Part I, pp 595-603, 1998.
- [2] Williams FW, Kennedy D, Butler R and Anderson MS. VICONOPT: program for exact vibration and buckling analysis or design of prismatic plate assemblies. *AIAA Journal*, Vol. 29, No. 11, pp 1927-1928, 1991.
- [3] Bruhn EF. *Analysis and design of flight vehicle structures*. 1st edition, S R Jacobs, 1973.
- [4] Wittrick WH and Williams FW. Buckling and vibration of anisotropic or isotropic plate assemblies under combined loading. *International Journal of Mechanical Sciences*, Vol. 16, No. 4, pp 209-223, 1974.
- [5] Anderson MS, Williams FW and Wright CJ. Buckling and vibration of any prismatic assembly of shear and compression loaded anisotropic plates with an arbitrary supporting structure. *International Journal of Mechanical Sciences*, Vol. 25, No. 8, pp 585-596, 1983.
- [6] Karman T von. *Enzyklopädie der Mathematischen Wissenschaften*. Vol. IV, p 349, 1910.